Draft version January 26, 2013
Preprint typeset using LaTeX style emulateapj v. 11/10/09

arXiv:1105.5486v1 [astro-ph.GA] 27 May 2011

A 100-PARSEC ELLIPTICAL AND TWISTED RING OF COLD AND DENSE MOLECULAR CLOUDS REVEALED BY *HERSCHEL*[*] AROUND THE GALACTIC CENTER.

S. Molinari[1], J. Bally[2], A. Noriega-Crespo[3], M. Compiègne[3], J. P. Bernard[4], D. Paradis[4], P. Martin[5], L. Testi[6,7], M. Barlow[8], T. Moore[9], R. Plume[10], B. Swinyard[8,11], A. Zavagno[12], L. Calzoletti[13], A. M. Di Giorgio[1], D. Elia[1], F. Faustini[13], P. Natoli[14], M. Pestalozzi[1], S. Pezzuto[1], F. Piacentini[15], G. Polenta[13], D. Polychroni[1], E. Schisano[1], A. Traficante[14], M. Veneziani[15], C. Battersby[2], M. Burton[16], S. Carey[3], Y. Fukui[17], J. Z. Li[18], S. D. Lord[19], L. Morgan[9], F. Motte[20], F. Schuller[21], G. S. Stringfellow[2], J. C. Tan[22], M. A. Thompson[23], D. Ward-Thompson[24], G. White[11,25], G. Umana[26]

Draft version January 26, 2013

ABSTRACT

Thermal images of cold dust in the Central Molecular Zone of the Milky Way, obtained with the far-infrared cameras on-board the Herschel satellite, reveal a $\sim 3 \times 10^7$ $M_\odot$ ring of dense and cold clouds orbiting the Galactic Center. Using a simple toy-model, an elliptical shape having semi-major axes of 100 and 60 parsecs is deduced. The major axis of this 100-pc ring is inclined by about 40° with respect to the plane-of-the-sky and is oriented perpendicular to the major axes of the Galactic Bar. The 100-pc ring appears to trace the system of stable x_2 orbits predicted for the barred Galactic potential. Sgr A* is displaced with respect to the geometrical center of symmetry of the ring. The ring is twisted and its morphology suggests a flattening-ratio of 2 for the Galactic potential, which is in good agreement with the bulge flattening ratio derived from the 2MASS data.

Subject headings: Galaxy: center — ISM: clouds

1. INTRODUCTION

Observations of the central regions of our Milky Way Galaxy provide the nearest template for the study of the conditions in galactic nuclei in normal galaxies. The 3.6×10^6 $M_\odot$ black hole at the center dominates the Central Molecular Zone (CMZ) which extends from Galactic longitude l = -1° to about +1.5° and hosts the densest and most massive molecular clouds in the Milky Way (Morris & Serabyn 1996). The CMZ may be a Galactic analog of the nuclear star-forming rings observed in the centers of star forming barred galaxies (Kormendy & Kennicutt 2004, Kormendy & Cornell 2004). The CMZ contains tens of millions of solar masses of cold interstellar matter (ISM) (Pierce-Price et al. 2000; Bally et al. 2010) and harbors several of its most active sites of star formation such as Sgr A, Sgr B2, and Sgr C (Yusef-Zadeh et al. 2008,Yusef-Zadeh et al. 2009). The gas kinematics and distribution of near-infrared light indicate that the gravitational potential in the inner Galaxy is dominated by a bar with a major axis inclined by about 20 to 45° with respect to our line-of sight (Binney et al. 1991, Benjamin et al. 2003, Minchev et al. 2007).

Despite the active star formation and bar dynamics, warm dust has been found to be a relative minor constituent in the CMZ. Sodroski et al. (1994) used COBE/DIRBE data to constrain dust properties in the CMZ and Rodríguez-Fernández et al. (2004) presented ISO observations. These studies found that 15 to 30% of the far-IR emission comes from molecular clouds with dust temperatures of about 19 K, 70 to 75% arises from the HI phase with dust temperatures of 17 to 22 K, and less than 10% is emitted by warm dust with T > 29 K associated with the extended HII and warm (100 to 300 K) molecular phases traced by H_3^+ absorption (Oka et al. 2005, Goto et al. 2008). With Herschel we can now extend this type of analysis into a new domain of spatial resolution and sensitivity.

In this Letter, we present the first high-angular resolution maps of the CMZ far-IR dust emission, temperature, and column density based on data obtained with the Herschel satellite (Pilbratt et al. 2010).

2. OBSERVATIONS AND RESULTS

The Galactic Center was observed with Herschel as part of the Hi-GAL Key-Project (the Herschel infrared Galactic Plane Survey, Molinari et al. 2010b). Observing strategy and basic data reduction are described in Molinari et al. (2010a)

[*] *Herschel* is an ESA space observatory with science instruments provided by European-led Principal Investigator consortia and with important participation from NASA.

[1] INAF-IFSI, Via Fosso del Cavaliere 100, I-00133 Roma, Italy
[2] CASA, University of Colorado, Boulder CO, USA 80309
[3] Spitzer Science Center, Caltech, 91125 Pasadena, USA
[4] CNRS, IRAP, F-31028 Toulouse cedex 4, France
[5] Department of Astron. & Astroph., University of Toronto, Canada
[6] ESO Headquarters, Garching, Germany
[7] INAF-Osservatorio Astrofisico di Arcetri, 50125 Firenze, Italy
[8] Department of Physics and Astronomy, UCL, London, UK
[9] Astrophysics Research Institute, Liverpool John Moores University, UK
[10] Department of Physics & Astronomy, University of Calgary, Canada
[11] STFC, Rutherford Appleton Labs, Didcot, UK
[12] LAM, Université de Provence, Marseille, France
[13] ASI Science Data Center, I-00044 Frascati, Italy
[14] Dipartimento di Fisica, Università di Roma "Tor Vergata", Roma, Italy
[15] Dipartimento di Fisica, Università di Roma "La Sapienza", Roma, Italy
[16] School of Physics, University of New South Wales, Australia
[17] Department of Astrophysics, Nagoya University, Nagoya, Japan
[18] NAO, Chinese Academy of Sciences, Beijing, China
[19] NASA Herschel Science Center, Caltech, 91125 Pasadena, USA
[20] Laboratoire AIM, CEA/DSM - INSU/CNRS - Université Paris Diderot, IRFU/SAp CEA-Saclay, 91191 Gif-sur-Yvette, France
[21] MPIfR-MPG, Bonn, Germany
[22] Departments of Astronomy & Physics, University of Florida, Gainesville, FL 32611, USA
[23] Centre for Astrophysics Research, Science and Technology Research Institute, University of Hertfordshire, Hatfield, UK
[24] School of Physics and Astronomy, Cardiff University, Cardiff, UK
[25] Department of Physics and Astronomy, The Open University, Milton Keynes, UK
[26] INAF-Osservatorio Astrofisico di Catania, Catania, Italy

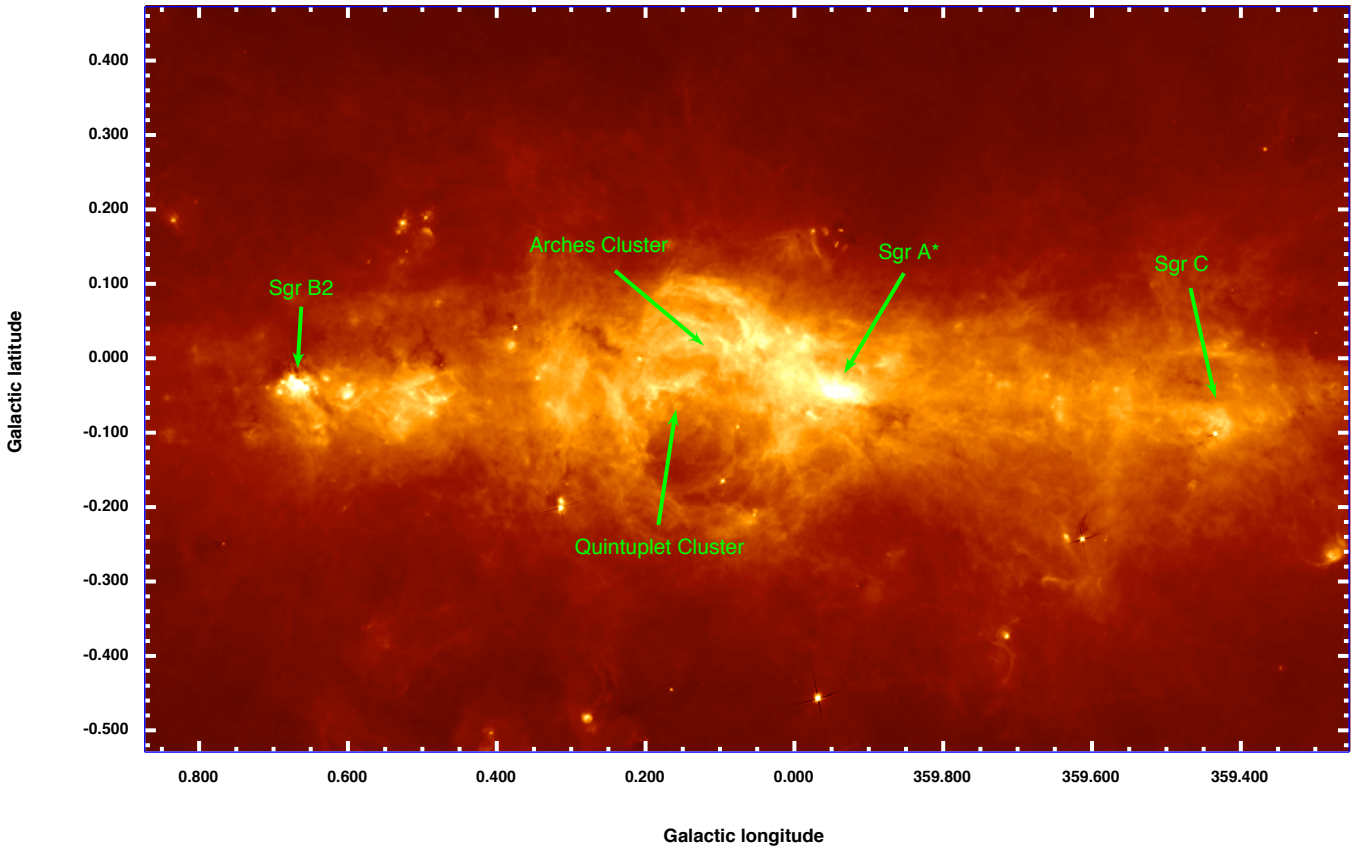

FIG. 1.— Herschel PACS 70 μm image of the Galactic Center region. Labels identify known objects that are discussed in the text.

and Traficante et al. (2011). The central 2°x2° region of the Galaxy was imaged in Parallel Mode by acquiring simultaneously PACS (Poglitsch et al. 2010) and SPIRE (Griffin et al. 2010) images in 5 photometric bands centered at 70, 160, 250, 350 and 500 μm. SPIRE was used in "bright-source mode", to minimize non-linearities and saturation in this very bright region; preliminary SPIRE calibration checks indicate an accuracy within 15% compared to standard SPIRE setting (M. Pohlen, priv. comm.). We corrected the zero-level in our SPIRE and PACS images using offset values derived from the comparison with the Planck/IRAS data using the same procedure as in Bernard et al. (2010).

Figure 1 shows the PACS 70 μm image. Sgr A* and Sgr B2 are the brightest spots, and the entire area is filled with intense far-IR emission punctuated by several InfraRed Dark Clouds (IRDCs) seen in silhouette. A large bubble dominates at 70 μm from $0° \lesssim l \lesssim +0.20°$ but disappears at longer wavelengths (see SPIRE 250 μm in fig. 2). At 250 μm Sgr B2 is the brightest feature (it is saturated at 250 μm). Two bent chains of emission extend above and below the mid-plane from Sgr B2 to Sgr A*, where they appear to cross, and continue on to Sgr C. This structure can also be identified in the SCUBA map (Pierce-Price et al. 2000), but only the unique multi-band far-IR/submm capabilities of the Herschel PACS and SPIRE cameras make possible the determination of its temperature and column density.

Opacity and dust temperature are estimated from a pixel-to-pixel fit to the 70-350 μm data (the resolution is matched to the 350 μm images – ~25″) using the DustEM model (Compiègne et al. 2011) following the method described in Bernard et al. (2010). Assuming constant dust properties, the opacity is converted into a hydrogen column density ($N_H = N_{HI} + N_{H_2}$) using $\tau_{250}/N_H = 8.8\,10^{-26}$ cm^2/H. This value is estimated from latitudes b>0, and it could be higher by a factor 2 - 4 in the Galactic plane (Bernard et al. 2010) and could change our mass estimates accordingly. The temperature and column density maps (Figs. 3 and 4) represent the integrated contribution of dust along the line of sight. High opacity, cold dust appears in silhouette against the warmer background even at 70 μm (fig. 1). Although the derived temperature might be underestimated, a temperature map without the 70 μm data provides similar results.

The detailed study of the great bubble visible in the 70 μm and the temperature maps (figs. 1 and 3) will be presented in a forthcoming paper. This Letter is dedicated to the analysis of the large-scale filaments visible in the far-IR (fig.2), that trace a continuous chain of cold and dense clumps ($T_{dust} \leq 20$ K; $N(H) > 2 \times 10^{23}$ cm^{-2}) organized along an ∞-shaped feature that dominates the image between the Sgr C complex at l = 359.4° and Sgr B2 at 0.7°. The total projected extent is ~1.4°, or about 180 pc, for a solar Galactocentric distance of 8.4 kpc (Reid et al. 2009). Warmer dust with relatively lower column density ($T_{dust} \geq 25$ K, $N(H) < 2 \times 10^{23}$ cm^{-2}) fills the interior of the ∞-shaped feature.

3. A 100-PARSEC ELLIPTICAL RING OF COLD AND DENSE MOLECULAR CLOUDS: THE X_2 ORBITS

The ∞-shaped feature in the temperature map in fig. 3 coincides with high-column density material ($N(H) \geq 2 \times 10^{23}$ cm^{-2}) organized in a continuous chain of irregular clumps (see fig. 4). Most of the cold, high column density clumps

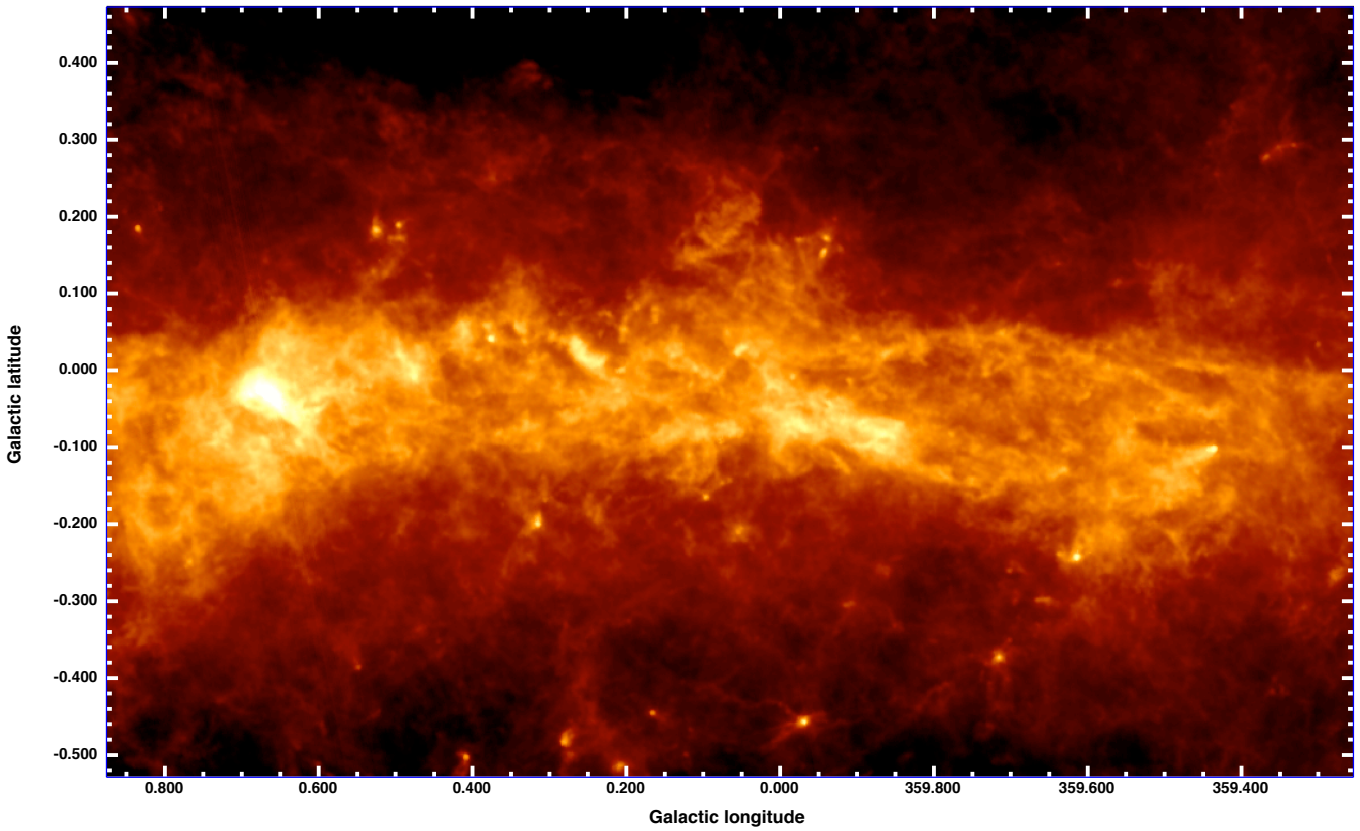

FIG. 2.— Herschel SPIRE 250 μm image of the Galactic Center region.

in the $[l^-, b^-]$ and $[l^+, b^+]$ arms of this feature are seen in silhouette against the 70 μm background (fig. 1); the same is not true for clumps along the $[l^+, b^-]$ and $[l^-, b^+]$ arms. We conclude that the $[l^-, b^-]$ and $[l^+, b^+]$ arms are in front of the bulk of the warmer dust emission (i.e. between us and the Galactic Center), while the $[l^-, b^-]$ and $[l^+, b^+]$ arms are located in the background.

We use the CS survey by Tsuboi et al. (1999) (their fig. 4) to extract the radial velocity of CS condensations positionally coincident with the cold and dense peaks on varius positions along the ∞-shaped feature in figs. 3 and 4. The position-velocity information is averaged in latitude bins of 1.5′, so the information can be extracted with some degree of approximation but should be adequate to represent the mean velocity of the various clouds and clumps. The full span of velocities found toward each position is reported in fig. 4.

The $[l^-, b^+]$ arm shows steadily increasing (in absolute values) negative velocities from the center of symmetry toward Sgr C indicating approaching material with increasing relative speed. Following the $[l^-, b^-]$ arm from Sgr C back to the centre we find negative velocities decreasing and changing to positive (receding) values at l ∼359.8°. Continuing along the $[l^+, b^+]$ arm the radial velocities are still positive and slowly increasing, indicating material receding at higher and higher speeds up to Sgr B2. Finally along the $[l^+, b^-]$ arm we see velocities decrease again going back toward the center of symmetry of the ∞-shaped feature. The distribution of radial velocities along the ∞-shaped feature seems to indicate an ordered, rotating pattern around its projected center of symmetry.

3.1. *A simple model for the ∞-shaped feature: a 100-pc elliptical twisted ring*

A simplified toy model of the ∞-shaped feature is built assuming that the material is distributed along an elliptical orbit (projected onto the Galactic Plane) with semi-axes $[a, b]$ and major-axis position angle θ_p. For simplicity, a constant orbital speed v_{orb} is assumed. An additional sinusoidal vertical oscillation component with a vertical frequency ν_z and a phase θ_z is added to the equations of the ellipse describing the orbit. Adopting a coordinate system with the x axis oriented toward negative longitudes, y axis pointing away along the line of sight from the Sun, and z axes toward positive latitudes (see Fig. 5), the position and radial velocity of each point along the orbit is described as a function of the polar angle θ_t (counter-clockwise from the x axes) as

$$\begin{cases} x = a\ \cos\theta_t\ \cos\theta_p - b\ \sin\theta_t\ \sin\theta_p \\ y = a\ \cos\theta_t\ \sin\theta_p + b\ \sin\theta_t\ \cos\theta_p \\ z = z_0\ \sin\nu_z(\theta_p - \theta_z) \\ v_r = -v_{orb}\ \cos(\theta_p + \theta_t) \end{cases}$$

We let a, b, θ_p and v_{orb} vary until they match the observed projected morphology of the ellipse and the distribution of radial velocities at 20 positions along the ∞-shaped feature. We keep z_0 fixed at 15 pc, which is half of the measured b-extent of the ∞-shaped feature; we also fix ν_z=2 in units of the orbital frequency, as indicated by the projected twist shape (see §3.3). The fitting procedure minimizes a pseudo-χ^2 value ξ

$$\xi = \sum_{i=1}^{20} \frac{(v_r - v_{obs})^2}{\Delta v_{obs}} \quad (1)$$

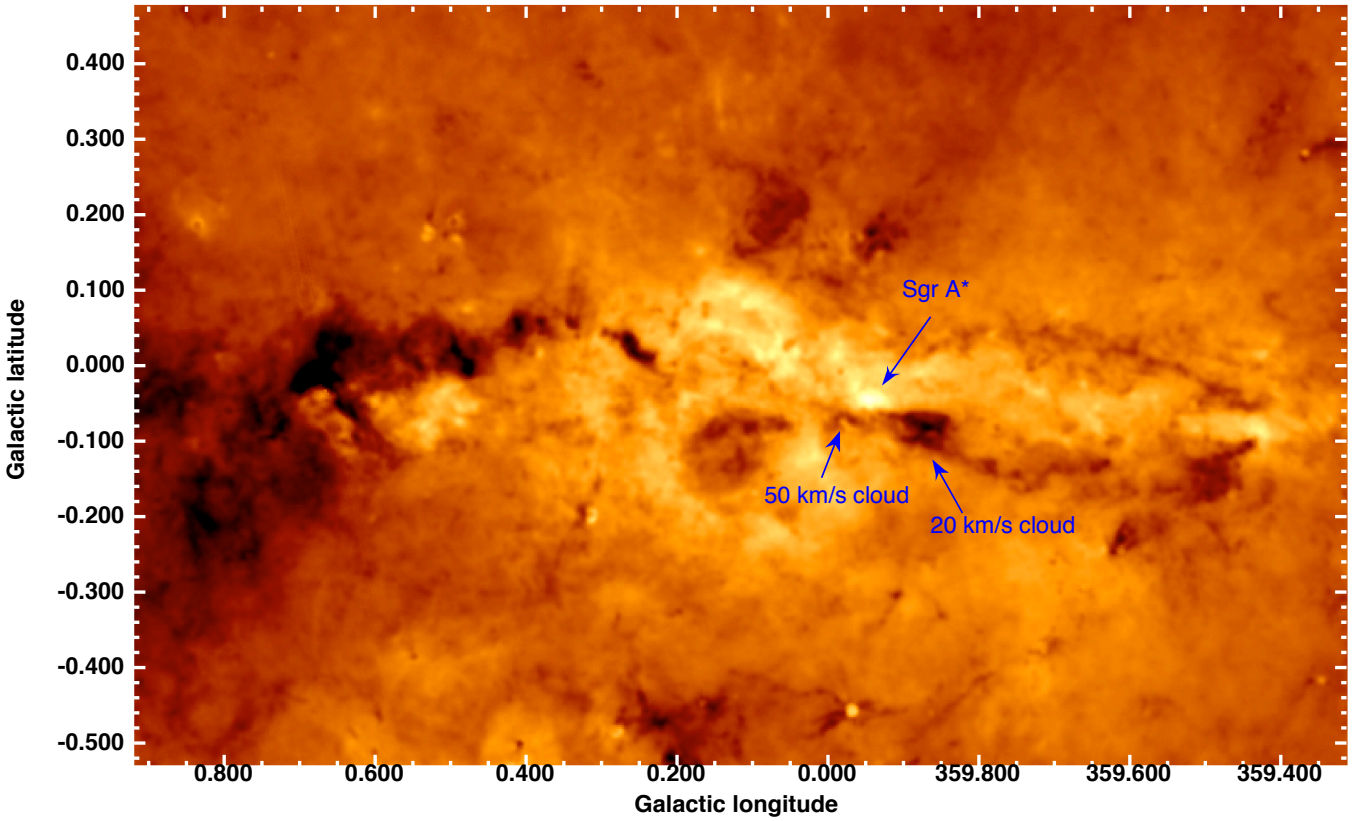

FIG. 3.— Temperature map of the Galactic Center region. The Log-color stretch extends from 15K to 40K on Sgr A*.

where Δv_{obs} is half of the velocity range toward each of the 20 test positions (see fig. 4).

The best fit is obtained for an ellipse with a = 100pc, b =60pc, θ_p = −40°, and v_{orb}=80 km s^{-1}; θ_z ~0 implying that the ring crosses the midplane along the X axes. These numbers should be taken with caution, as the velocities are derived by eye from a plot. However, the discrepancy between the model radial velocity and the observed ones is within ±25 km s^{-1}. The only exception is the 50 km s^{-1} cloud (see fig. 3) located close in projection to Sgr A* (see §3.2).

The CMZ has been the subject of many studies in millimeter molecular tracers, and although the interpretation is difficult for the extreme confusion along the line of sight, several features were identified. Sofue (1995) analysed the CO data in Bally et al. (1987) and identified two large-scale structures (the "Arms"). Tsuboi et al. (1999) recognized a large-scale feature in their CS position-velocity diagram, that they call "Galactic Center Bow" which matches the $[l^-, b^-]$-$[l^+, b^+]$ arms of the ∞-shaped feature. The cold, high column-density dust features identified in the Herschel images, used as a proxy for the densest molecular gas, now indicate that the previously identified "Arms" and the "Galactic Center Bow" are parts of a single, twisted and elliptical ring rotating around Sgr A*. Figure 5 presents a sketch of the proposed arrangement of what we will call the100-pc ring.

A rough estimate of the ring mass is obtained by integrating the N(H) map within a contour surrounding the 100-pc ring which encloses material with N(H) $\gtrsim 2 \times 10^{23}$ cm^{-2} (for a corresponding solid angle of $\sim 4 \times 10^{-5} sr$). The contribution of background or foreground gas is removed by subtracting a column density of N(H) = 2×10^{23} cm^{-2}, the mean N(H) value in the interior of ∞-shaped feature. The resulting ring mass is $\sim 3 \times 10^7$ M$_\odot$ (it is $\sim 4 \times 10^7$ M$_\odot$ without background subtraction). Within the uncertainties, the derived ring mass agrees with 5.3×10^7 M$_\odot$ estimated from SCUBA maps (Pierce-Price et al. 2000) and 3×10^7 M$_\odot$ from CO data (Dahmen et al. 1998).

The 100-pc ring traces gas and dust moving about the nucleus on an elliptical orbit whose major axis (the straight red line in the right panel of fig. 5) is perpendicular to the major axis of the great Galactic bar, oriented 20 to 45° with respect to our line-of-sight (see fig. 5). The 100-pc ring is likely located on the so-called 'x_2' orbit system, which precesses at the same rate as the solid-body angular velocity of the Galactic Bar, resulting in stable, non-intersecting trajectories (Binney et al. 1991). These x_2 orbits are enclosed within another larger system of stable orbits, called x_1, elongated along the Galactic Bar. The prominent Sgr B2 and Sgr C star-forming complexes are located at the two projected longitude extrema of the 100-pc ring where gas on x_1 and x_2 orbits may collide, producing strong shocks which may trigger the formation of massive molecular cloud formation as well as enhanced star formation rates by the shock focusing mechanism suggested by Kenney & Lord (1991) for the spiral-bar interface of M83.

It is tempting to speculate that the 100-pc ring constitutes the remnant of a more persistent dusty torus that may have played a role in past AGN phases of our Galaxy. The recent Fermi-LAT detection of a large gamma-ray bubble emanating from the Galactic Center (Su et al. 2010, Crocker 2011, Zubovas et al. 2011) provides possible evidence for such past activity. Mid-IR interferometry of AGNs reveals compact dusty structures with a radius of a few parsecs, (e.g. Jaffe et al.

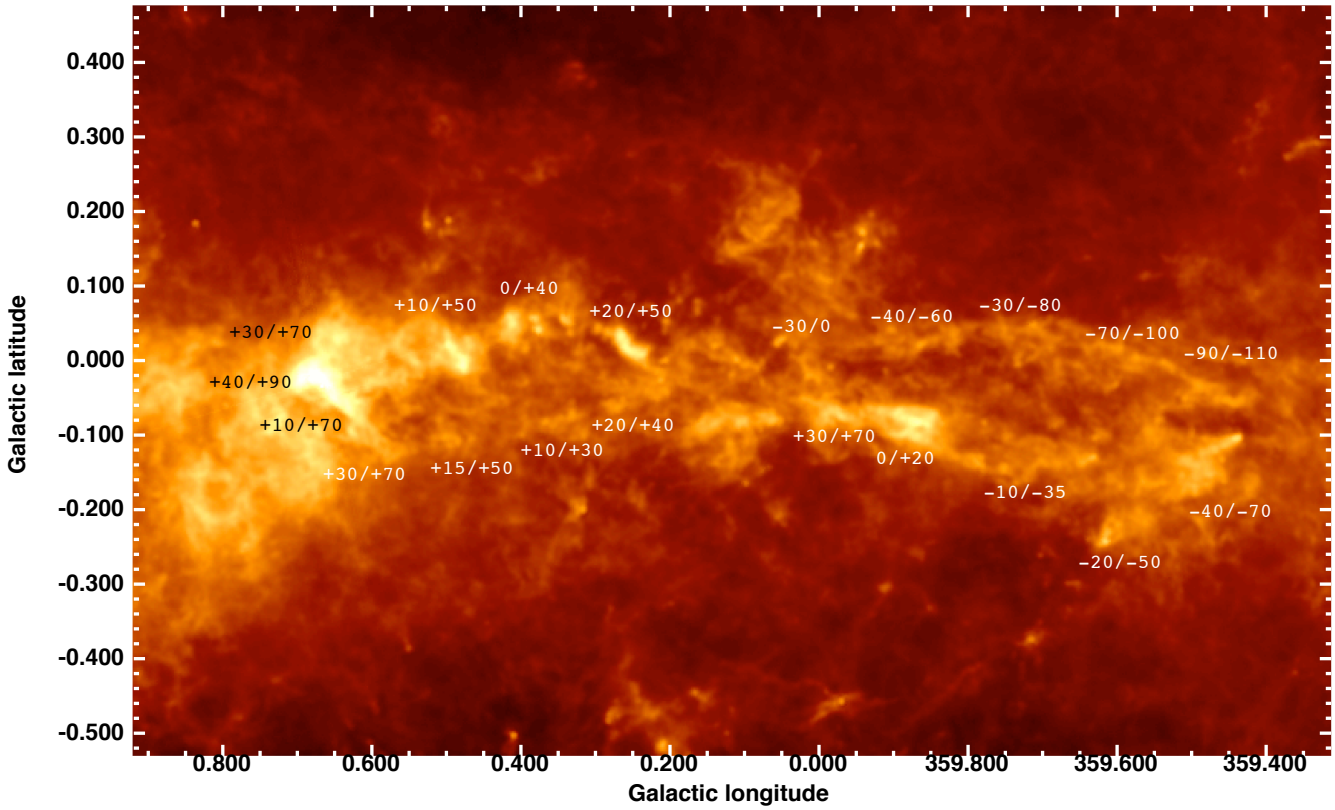

FIG. 4.— Atomic hydrogen column density map of the Galactic Center region. Color scale shown is logarithmic and extends from 4×10^{22} cm^{-2} in the dark regions, to 4×10^{25} cm^{-2} in the brightest region corresponding to Sgr B2. Velocity information is extracted from CS spectroscopic cubes (Tsuboi et al. 1999) for the gas counterparts positionally associated with the dense dust clumps; the range values indicate the range where emission is observed.

2004, Radomski et al. 2008), but there is additional evidence from Spitzer imaging and spectroscopy suggesting that larger and more persistent structures play a role in shaping observed AGN properties (e.g. Shi et al. 2006, Quillen et al. 2006). Model predictions (e.g. Krolik 2007) for torus column density in excess of 10^{24} cm^{-2}, and orbital speed $\sim$100 km s^{-1}, seem to be consistent with the parameters we estimate for the 100-pc ring.

3.2. *The relation between the 100-pc ring and Sgr A**

Sgr A*is noticeably displaced $\sim 10'$ (24 pc in projection) towards the negative longitude side of the geometrical center of symmetry of the 100-pc ring. The ring displacement with respect to the supposed location of the Galactic Center is consistent with the overall displacement of dense gas within the CMZ. Two-thirds to three-quarters of the cold interstellar gas and dust within the inner few hundred parsecs of the nucleus is at positive longitudes with respect to Sgr A*(Bally et al. 1988, Morris & Serabyn 1996). A similar asymmetry is present in the observed radial velocity on the 100-pc ring close to the location of Sgr B2, as opposed to Sgr C (see fig. 4). This may indicate an additional pattern motion of $\sim 10 - 20$ km s^{-1} of the 100-pc ring as a whole along its major axes and toward us, implying a 'sloshing' motion back and forth that could be explained as the response of the gas to an m=1 mode in the Galactic bar potential (Morris & Serabyn 1996).

The projected proximity of the 20 and 50 km s^{-1} clouds to Sgr A*, has led to the suggestion (e.g. Herrnstein & Ho 2005) that they are physically interacting with Sgr A*. If they are part of the 100-pc ring, then Sgr A* must be closer to the front of the ring than to its back; Sgr A* may then not be in the ring center, nor lie along the ellipses axes. Proximity to Sgr A* could be the source of the roughly 40 km s^{-1} deviation of the radial velocity of the 50 km s^{-1} cloud from the value predicted by the model of the rotating elliptical ring.

Given the extent of the 100-pc ring, its orbital motion is driven by the enclosed gas and bulge stars. If, however, ring material passes in proximity of Sgr A* the gravitational pull due to the strong mass concentration can be substantial. Indeed, the 3.6×10^6 M$_\odot$ black hole in Sgr A* dominates the gravitational potential only to a radius of a few parsecs. Beyond that distance the potential is dominated by the stellar mass in the bulge with a radial density profile of the form $\rho(r) \approx \rho_0(r/r_b)^{-\alpha}$ where $\alpha \approx -1.9$, $r_b \sim 0.34$pc and $\rho_0 \sim 2.1 \times 10^6$ M$_\odot$/pc^3 (Trippe et al. 2008). We then treat the gravitational pull from the Sgr A* mass concentration as an additional component over the general rotational motion. Using Newton's 2nd law:

$$\frac{GM_C(r)}{r^2} = \frac{\Delta \mathrm{v}}{t_0} \qquad (2)$$

where r is the distance between Sgr A* and the two molecular clouds (that is assumed similar for the two clouds if they belong to the 100-pc ring), $M_C(r)$ is the mass enclosed in a sphere of radius r centered on Sgr A* and t$_0$ is the timescale for the cloud passing in front of Sgr A*. The latter can be written as $t_0 = \Delta x/\mathrm{v}_{orb}$, where Δx is the projected distance between the 50 and 20 km s^{-1} clouds and v_{orb} is their orbital speed. Eq. 2 can then be rewritten

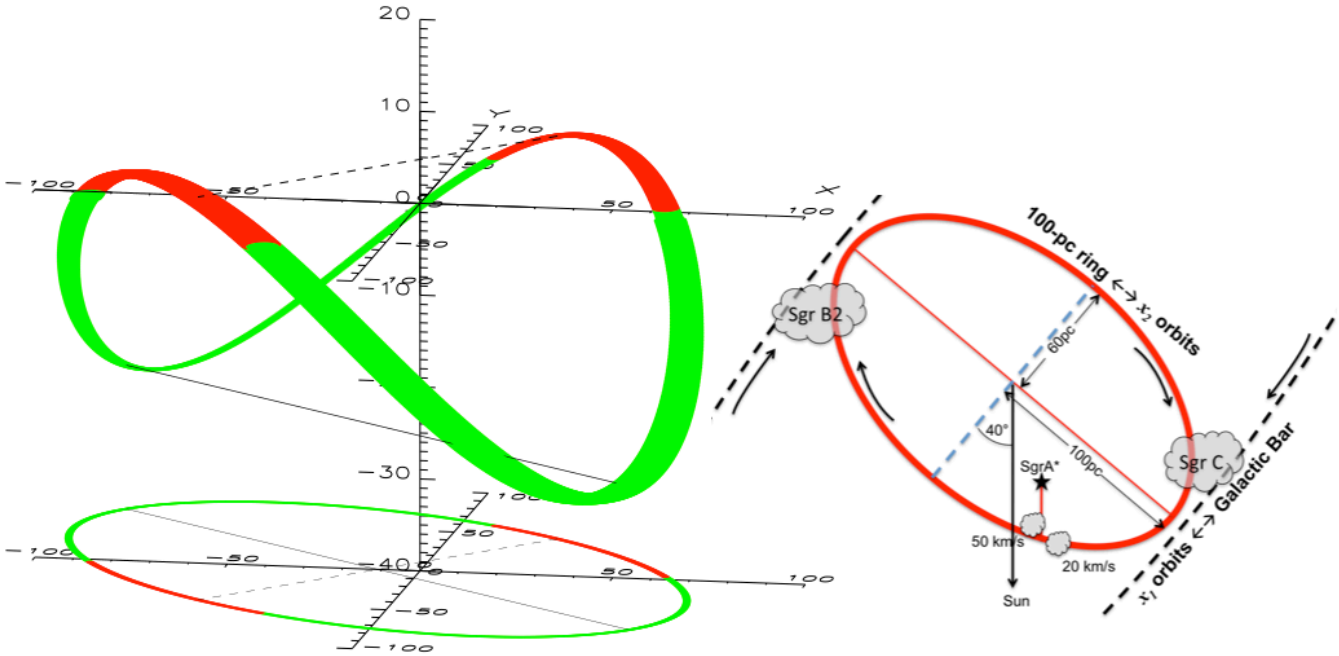

FIG. 5.— Sketch of the proposed 3D structure and placement of the 100-pc ring. *Left panel:* the ring is represented by the thick color line (red and green mark positions above and below b=0°. The line of sight to the Sun is along the Y axes. The thin full and dashed lines represent the major and minor axes of the ellipse. *Right panel:* Top view of the 100-pc ring with the proposed location of major clouds. The thick black dashed lines represent the innermost x_1 orbits. The position of SgrA* along the line of sight is the one corresponding to the distance it should have from the front portion of the 100-pc ring to justify the velocity difference between the 20 and 50 km s^{-1} clouds if due to the gravitational pull of the mass concentration around Sgr A* (see text).

$$r = \sqrt{\frac{GM_C(r)\Delta x}{\Delta \mathrm{v}\, \mathrm{v}_{orb}}} \tag{3}$$

Using this formulation to estimate $M_C(r)$, the measured projected distance between the nearest edges of the two clouds of $\Delta x \sim 7$pc, and assuming an orbital speed of 80km s^{-1} from our toy model fit, Eq. 3 provides $r \sim 20$ pc. In other words, to explain the difference in radial velocities between the 20 and 50 km s^{-1}clouds would require that Sgr A* is closer than 20pc to the foregreound arm of the 100-pc ring.

3.3. *The ring's twist: constraints on the flattening of the Galactic potential*

Perhaps the most striking aspect of the 100-pc ring is its twist. Apparently the gas in the ring oscillates twice about the mid-plane each time it orbits the nucleus once. Assuming the elliptical axes and the orbital speed derived from the toy model, the orbital period is $P_o \sim 3 \times 10^6$ years; the period of the vertical oscillations is therefore $P_z \sim 1.5 \times 10^6$ years. The coherence of the ring's morphology suggests stability over a few revolutions. Thus, the relationship between P_o and P_z can be used to infer constraints on the flattening of the gravitational potential in the CMZ. Assuming as a gross approximation that the matter (gas and stars) is distributed in a uniform-density ρ_0 slab of thickness h, P_o at a distance R can then be expressed as

$$P_o = \sqrt{\frac{4\pi R}{G\rho_0 h}} \tag{4}$$

A perturbation on a particle rotating in the flattened slab potential will result, in a 1st-order approximation (Binney & Tremaine 1987), in a harmonic oscillation both in radial and vertical directions. The vertical oscillation frequency can be expressed as

$$\nu_z^2 = \left(\frac{\partial^2 \Phi}{\partial z^2}\right)_{R,0} \tag{5}$$

The gravitational field along the z direction of the slab (approximated as infinite) is

$$F_z = 2\pi\rho_0 G h \tag{6}$$

so that the period of the vertical oscillations is

$$P_z = \sqrt{\frac{2\pi}{\rho_0 G}} \tag{7}$$

As noted above, the ∞ shape that the ring displays in projection implies that

$$P_o = 2P_z \tag{8}$$

or, using Eqs. 4 and 7,

$$h = \frac{R}{2} \tag{9}$$

The shape of the 100-pc ring would therefore imply a flattened potential in the CMZ that is consistent with a $x/z = 0.5$ axial ratio bulge mass distribution, remarkably similar to the value of 0.5–0.6 recently derived (Rodriguez-Fernandez & Combes 2008) fitting the 2MASS data to a potential model that includes the bulge and the nuclear bar.

4. CONCLUSIONS

The far-infrared multi-band images provided by the Hi-GAL survey using the Herschel PACS and SPIRE cameras provide evidence for a 100x60 parsecs elliptical ring of cold and dense clouds orbiting around the Galactic Center on x_2 orbits elongated along the minor axis of the Galactic center Bar. The ring is twisted with a vertical frequency that is twice the orbit frequency, indicating a flattening-ratio of 2 for the Galactic Center gravitational potential, consistent with the value derived from bulge star 2MASS number counts.

Data processing has been possible thanks to ASI support via contract I/038/080/0. We thank the referee, M. Morris, whose comments led to a more focused paper. We thank L. Spinoglio, N. Sacchi and A. Marconi for useful discussions on AGNs, and M. Pohlen and the SPIRE ICC for the preliminary analysis of the SPIRE "bright source mode" calibration.

REFERENCES

Bally, J., Aguirre, J., Battersby, C., Bradley, E. T., Cyganowski, C., & et al. 2010, ApJ, 721, 137
Bally, J., Stark, A. A., Wilson, R. W., & Henkel, C. 1987, ApJS, 65, 13
—. 1988, ApJ, 324, 223
Benjamin, R. A., Churchwell, E., Babler, B. L., Bania, T. M., Clemens, D. P., Cohen, M., Dickey, J. M., Indebetouw, R., Jackson, J. M., Kobulnicky, H. A., Lazarian, A., Marston, A. P., Mathis, J. S., Meade, M. R., Seager, S., Stolovy, S. R., Watson, C., Whitney, B. A., Wolff, M. J., & Wolfire, M. G. 2003, PASP, 115, 953
Bernard, J. P., Paradis, D., Marshall, D. J., Montier, L., Lagache, G., & et al. 2010, A&A, 518, L88
Binney, J., Gerhard, O. E., Stark, A. A., Bally, J., & Uchida, K. I. 1991, MNRAS, 252, 210
Binney, J. & Tremaine, S. 1987, Galactic Dynamics (Princeton Series in Astrophysics)
Compiègne, M., Verstraete, L., Jones, A., Bernard, J.-P., Boulanger, F., & et al. 2011, A&A, 525, 103
Crocker, R. M. 2011, in Proceedings of the 25th Texas Symposium on Relativistic Astrophysics (Heidelberg, 2010)
Dahmen, G., Huttemeister, S., Wilson, T. L., & Mauersberger, R. 1998, A&A, 331, 959
Goto, M., Usuda, T., Nagata, T., Geballe, T. R., McCall, B. J., & et al. 2008, ApJ, 688, 306
Griffin, M. J., Abergel, A., Abreu, A., & et al. 2010, A&A, 518, L3
Herrnstein, R. M. & Ho, P. T. P. 2005, ApJ, 620, 287
Jaffe, W., Meisenheimer, K., Röttgering, H. J. A., Leinert, C., Richichi, A., & et al. 2004, Nature, 429, 47
Kenney, D. P. & Lord, S. D. 1991, ApJ, 381, 118
Kormendy, J. & Cornell, M. E. 2004, Penetrating Bars Through Masks of Cosmic Dust, Vol. 319, p. 261 (Kluwer Academic Publishers)
Kormendy, J. & Kennicutt, Jr., R. C. 2004, ARA&A, 42, 603
Krolik, J. H. 2007, ApJ, 661, 52
Minchev, I., Nordhaus, J., & Quillen, A. C. 2007, ApJ, 664, L31
Molinari, S., Faustini, F., Schisano, E., Pestalozzi, M., & Di Giorgio, A. 2010a, A&A submitted
Molinari, S., Swinyard, B., Bally, J., Barlow, M., Bernard, J., Martin, P., Moore, T., Noriega-Crespo, A., Plume, R., Testi, L., Zavagno, A., & et al. 2010b, PASP, 122, 314
Morris, M. & Serabyn, E. 1996, ARA&A, 34, 645
Oka, T., Geballe, T. R., Goto, M., Usuda, T., & McCall, B. J. 2005, ApJ, 632, 882
Pierce-Price, D., Richer, J. S., Greaves, J. S., Holland, W. S., Jenness, T., & et al. 2000, ApJ, 545, L121
Pilbratt, G., Riedinger, J. R., Passvogel, T., & et al. 2010, A&A, 518, L1
Poglitsch, A., Waelkens, C., Geis, N., & et al. 2010, A&A, 518, L2
Quillen, A. C., Brookes, M. H., Keene, J., Stern, D., Lawrence, C. R., & Warner, M. W. 2006, ApJ, 645, 1092
Radomski, J. T., Packham, C., Levenson, N. A., Perlman, E., Leeuw, L. L., & et al. 2008, ApJ, 681, 141
Reid, M. J., Menten, K. M., Zheng, X. W., Brunthaler, A., Moscadelli, L., & et al. 2009, ApJ, 700
Rodriguez-Fernandez, N. J. & Combes, F. 2008, A&A, 489, 115
Rodríguez-Fernández, N. J., Martín-Pintado, J., Fuente, A., & Wilson, T. L. 2004, A&A, 427, 217
Shi, Y., Rieke, G. H., Hines, D. C., Gorjian, V., Werner, M. W., & et al. 2006, ApJ, 653, 127
Sodroski, T. J., Bennett, C., Boggess, N., Dwek, E., Franz, B. A., Hauser, M. G., Kelsall, T., Moseley, S. H., Odegard, N., Silverberg, R. F., & Weiland, J. L. 1994, ApJ, 428, 638
Sofue, Y. 1995, PASJ, 47, 527
Su, M., Slayter, T. R., & Finkbeiner, D. P. 2010, ApJ, 724, 1044
Traficante, A., Calzoletti, L., Veneziani, M., & et al. 2011, MNRAS, accepted
Trippe, S., Gillessen, S., Gerhard, O., Bartko, H., Fritz, T., Maness, H., Eisenhauer, F., Martins, F., Ott, T., Dodds-Eden, K., & Genzel, R. 2008, A&A, 492, 419
Tsuboi, M., Handa, T., & Ukita, N. 1999, ApJ Suppl. Ser., 120, 1
Yusef-Zadeh, F., Braatz, J., Wardle, M., & Roberts, D. 2008, ApJ, 683, L147
Yusef-Zadeh, F., Hewitt, J. W., Arendt, R. G., Whitney, B. A., Rieke, G., & et al. 2009, ApJ, 702, 178
Zubovas, K., King, A. R., & S., N. 2011, MNRAS accepted, arXiv:1104.5443